Structural and antibacterial properties of AgFe₂O₄ and Fe₃O₄ nanoparticles, and their nanocomposites

Azam Hashemi[a], Hadis Tavafi[b]*, Mahmoud Naseri[a]*, Hossein Mojtabazadeh[c], Mina Abedi[d], Narges Tork[e]

[a]Department of Physics, Faculty of Science, Malayer University, Malayer, Iran
[b]Department of Biology, Faculty of Science, Malayer University, Malayer, Iran
[c]Department of Organic Chemistry, Faculty of Chemistry, University of Kashan, Kashan, Iran
[d]Department of Chemistry, Islamic Azad University Central Tehran Branch, Iran
[e]Department of Biology, Faculty of science, Razi University, Kermanshah, Iran

ARTICLE INFO

ABSTRACT

This research investigated the antibacterial activities of AgFe₂O₄ and Fe₃O₄ ferrite nanoparticles compared to AgFe₂O₄/SiO₂/Passiflora Caerulea and Fe₃O₄/SiO₂/Passiflora Caerulea nanocomposites. To synthesize ferrite nanocomposites, Passiflora Caerulea plant extract was doped onto ferrite nanoparticles with the assistance of silica (SiO₂). The degree of crystallinity, phase composition, microstructure, and the compositions of the samples were determined using X-ray diffraction (XRD), Fourier transform infrared (FT-IR) spectroscopy, field emission scanning electron microscopy (FESEM), and energy dispersive X-ray analysis (EDXA), respectively. Furthermore, the broth microdilution method was employed against Gram-positive and Gram-negative bacteria to assess the antimicrobial activity. The method was also applied to Gram-positive and Gram-negative bacteria to examine the antimicrobial activity. The results of the Minimum Inhibitory Concentration (MIC) and Minimum Bactericidal Concentration (MBC) of silver and iron nanocomposites indicated that these nanocomposites exhibited superior antibacterial activity compared to silver and iron ferrite nanoparticles. Thus, silver and iron ferrite nanocomposites could serve as a novel antibacterial agent against infectious bacteria.

1. Introduction

Nanotechnology is a rapidly growing field of modern research that focuses on synthesizing particles within the size range of approximately 1 to 100 nm. Within this size range, all aspects - chemical, physical, and biological - undergo significant changes compared to their bulk counterparts and individual atoms/molecules. Nanoparticles and nanomaterials are increasingly being utilized across various fields due to their enhanced properties attributed to size, biocompatibility, and morphological distribution [1]. Nanomaterials display special attributes such as catalytic, mechanical, optical, and biological properties, allowing for their application in a diverse array of areas. The high surface area, scattering, biocompatibility, and antibacterial properties of metal and metal oxide nanoparticles have led to their widespread use in fields including electrochemistry, medical devices, cosmetics, hygiene products, textiles, and more [2]. Iron oxide, among nanomaterials, has been extensively studied and approved by the Food and Drug Administration (FDA) as a nanomedicine. Magnetic iron oxide nanomaterials composed of magnetite (Fe₃O₄) or maghemite (Fe₂O₃) have demonstrated efficacy as drug delivery vehicles, contrast agents, and thermal-based therapeutics within specific diameters ranging from 15 nm to 100 nm [3]. Silver and its

compounds possess attractive properties, notably strong inhibitory and antibacterial effects, along with broad-spectrum antimicrobial activities against bacteria, fungi, and viruses. Silver's higher toxicity towards microorganisms compared to other metals has made it a valuable component in combating drug-resistant pathogens [4]. To address the challenges posed by drug-resistant pathogens, the synthesis of new compounds with antimicrobial activity is of paramount importance in medicine. Various studies have explored the antimicrobial effects of silver nanoparticles and their derivatives using different methods. While the disk diffusion method is commonly employed to test antibacterial properties, its limitations reduce sensitivity in antimicrobial investigations, highlighting the need for alternate techniques such as the broth microdilution method, known for its ease, speed, cost-effectiveness, and high sensitivity in antimicrobial studies [5]. Meanwhile, many previous reports pointed out that in 2019, Aritonang et al. synthesized silver nanoparticles using the aqueous extracts of Impatiens balsamina and Lantana camera plants to investigate their antibacterial effects. The study demonstrated that the extracts containing silver nanoparticles exhibited growth inhibitory activity against E. coli and Staphylococcus aureus bacteria [6]. Gong et al. conducted a study in 2007 in which they investigated the MIC of $AgFe_3O_4$ nanoparticles against E. coli, S. aureus, and B. subtilis bacteria using the microdilution method in a flask. The researchers reported that the nanoparticles displayed a significant antimicrobial effect [7]. Furthermore, in 2019, Lagashetti et al. synthesized a silver nanocomposite and evaluated its antibacterial impact using the disc diffusion method. Their findings revealed that the nanocomposite exhibited a moderate effect against E. coli, E. faecalis, and P. aeruginosa bacteria [8]. In 2020, Muthukumar et al. synthesized silver ferrite nanoparticles using a plant extract and compared their antibacterial efficacy to chemically synthesized nanoparticles. The study indicated that the plant-extract-synthesized nanoparticles demonstrated superior antibacterial effects against E. coli and S. aureus compared to chemically synthesized counterparts [9]. In 2023, Manimaran synthesized iron oxide nanoparticles using Pleurotus citrinopileatus extract, examined their antibacterial activity, and demonstrated a significant antibacterial effect against both gram-positive and gram-negative bacteria [10]. Furthermore, in 2020, Jamzad and colleagues synthesized iron oxide nanoparticles utilizing the aqueous extract of Laurus nobilis leaves through the green synthesis method, and after investigating their antimicrobial activity, reported that the synthesized nanoparticles had a moderate effect on Listeria monocytogenes [11]. This study aims to investigate the antimicrobial activity of silver and iron ferrite nanoparticles and their nanocomposites against bacterial pathogens with the goal of developing these synthesized nanoparticles as effective antibacterial agents replacing drug-resistant pathogens in medical applications [12]. Techniques such as combination of chemical and physical methods, laser ablation, hydrothermal, sol–gel, precipitation methods, electrodeposition technique, atomic force microscopy nanolithography, vapor phase transport method are commonly used in synthesizing nanomaterials [13-19].

Among these techniques, the thermal treatment method stands out as one of the best methods for producing ferrite nanostructures due to its environmentally friendly nature and relatively short processing time [20, 21]. In this work, $AgFe_2O_4$, and Fe_3O_4 synthesized using thermal treatment method. Furthermore, in the green synthesis of ferrite nanocomposites, Passiflora Caerulea plant extract is incorporated onto ferrite nanoparticles with the assistance of silica.

In short, the reason for using the selected materials is that these compounds consist of silver ferrite ($AgFe2O4$) and iron ferrite ($Fe3O4$). Silver ferrite nanoparticles are renowned for their potent antibacterial properties, as they can disrupt the cell membranes of bacteria and inhibit their growth. Conversely, iron oxide nanoparticles can enhance the antimicrobial activity of silver nanoparticles and contribute to the stability of the composition [22]. In addition, research results show that (Fe_3O_4) nanoparticles, due to their excellent stability, biocompatibility, and controllable sizes which help them to penetrate cells, can be useful in biomedical applications [23]. (Fe_3O_4) nanoparticles also act as electron donors due to the presence of Fe^{+2} states [24]. SiO_2: This denotes silicon dioxide nanoparticles, commonly referred to as silica. Silica nanoparticles are frequently employed as stabilizing agents in composite materials, enhancing the dispersion and stability of other nanoparticles. In this study, SiO_2 is included to boost the performance and overall efficacy of the composition [25].

Passiflora Caerulea: Also known as the blue passionflower, Passiflora Caerulea is a plant recognized for containing various bioactive compounds, such as flavonoids and alkaloids, which have demonstrated antibacterial properties in prior research. This ingredient is incorporated to introduce additional antibacterial effects and augment the overall antimicrobial activity [26].

The rationale behind combining these ingredients is to harness a synergistic effect that amplifies the antibacterial properties of the composite. By amalgamating silver nanoparticles for their robust antibacterial effects, iron oxide nanoparticles for enhanced stability and activity, silica nanoparticles for improved dispersion and stability, and Passiflora Caerulea for supplementary bioactive compounds, our objective is to develop a potent antibacterial agent.

2. Materials and method

2.1. Materials

Materials and compounds used in this article include deionized water as a solvent, Polyvinylpyrrolidone (PVP, Mw = 31000, Merck) as a stabilizing agent and preventing aggregation of particles, Iron nitrate, Fe $(NO_3)_3 \bullet 9H_2O$, and silver nitrate, $AgNO_3$, were purchased from Acros Organics (99%). Tetraethyl Orthosilicate (TEOS) and Ethanol (96%) were purchased from Sigma Aldrich. All other chemicals and reagents were of the analytical grade and employed without any additional purification with a purity above 99%.

2.2. synthesis of AgFe$_2$O$_4$ and Fe$_3$O$_4$ nanoparticles

To synthesize iron and silver ferrite nanoparticles, at first, 4 grams of poly vinyl pyrrolidone (PVP) was dissolved in 100 ml of deionized water at a temperature of 353K. Mechanism of interaction of PVP and metal ions in synthesize of metal ferrite nanoparticles, is as follows:

Generally, metal ions are linked by strong ionic bonds to the amide group of the polymer chain. PVP acts as a stabilizer for soluble metal salts through steric and electrostatic stabilization of the amide groups of the pyrrolidone ring and the methylene group. Initially, the PVP stabilizer can degrade to a limited extent, thus creating a shorter polymer chain and is blocked when adsorbed on the surface of metal ions. Metal ions, well dispersed in cavities and networks, are produced by shorter polymer chains [27]. The influence of PVP is not limited to the solution treatment and drying stages; PVP also affects the nucleation of metal ferrite nanoparticles during the calcination step. In this step, small nanoparticles with a high surface energy level will become larger due to Ostwald ripening without the presence of PVP, thereby breaking the steric barrier and thus preventing capacitors from their agglomeration. Using this technique, ferrite nanoparticles can be produced with proper stoichiometric control and uniform particle size distribution in a relatively short time at low temperatures [28]. Then, 0.2 mmol of iron nitrate and 0.1 mmol of silver nitrate (Fe:Ag = 2:1) were mixed, poured into the polymer solution, and stirred continuously for 2 hours using a magnetic stirrer. The mixture was then dried for 24 hours at 80°C in an oven. The resultant dried solid was crushed, and the resulting powder was calcined at 550°C for 3 hours.

2.3. Preparation and Synthesis of SiO2 Nanoparticles Using Passiflora Caerulea Plant Extract

In the first step, 100 ml of 96% ethanol and 35 ml of deionized water were mixed, and 16 ml of TEOS was added to the solution. The second step involved extracting 100 grams of Passiflora caerulea plant using a Soxhlet apparatus with a water-ethanol solvent (50:50) for 7 hours. The resulting extract was cooled to room temperature and used immediately. In the third step, the mixture from the first step was heated to 70°C using a heater stirrer, and 30 ml of the herbal extract obtained in the second step was added to it. The resulting mixture was then removed from the heater and cooled to room temperature, resulting in a colloidal solution of SiO$_2$. This method is known as a green method, and the same extract was used in all three steps, totaling 500 ml of extract used on the same day.

2.4. Green Synthesis of AgFe$_2$O$_4$/SiO$_2$ and Fe$_3$O$_4$/SiO$_2$ Nanocomposites

To prepare the AgFe$_2$O$_4$/SiO$_2$ nanocomposite, 1 gram of AgFe$_2$O$_4$ nanoparticle was placed in a balloon under nitrogen gas. Subsequently, 10 ml of SiO$_2$ colloidal solution was added to the mixture and stirred at room temperature for 8 hours under nitrogen gas. Following this, the stirrer was halted, and the mixture was stirred for an additional half an hour at room temperature without nitrogen. The resulting mixture was then centrifuged at 12,000 rpm for 10 minutes, and the precipitate was separated with

deionized water and washed once (20 ml). Finally, the mixture was dried in a vacuum oven without heat for 5 hours and then dried in a vacuum desiccator under calcium chloride. It is important to note that ferrite compounds are highly oxidizing, so nitrogen gas was utilized during the reaction time to prevent further oxidation. Moreover, no heat was applied to reduce the reactivity of the material, and the mixture was dried under calcium chloride to prevent oxidation. All these steps were repeated for Fe$_3$O$_4$/SiO$_2$ nanocomposites under the same conditions.

2.5. Antimicrobial Activity

The study utilized bacterial strains of Staphylococcus aureus (ATCC 6538), Streptococcus pyogenes (ATCC 19615), Escherichia coli (ATCC 8739), and Pseudomonas aeruginosa (ATCC 27853) obtained from the Iranian Biological Resource Center (IBRC) to investigate the antimicrobial activity of silver and iron ferrite nanoparticles and their nanocomposites. Each bacterial strain was cultured in MHA culture medium, and subsequently, a bacteria stock was prepared using 50% glycerol and stored at -20°C for antibacterial experiments. The antimicrobial effects of silver ferrite nanoparticles and their nanocomposites were evaluated using the microdilution method in microtiter plates. The minimum growth inhibitory concentration (MIC) was determined in accordance with the CLSI M100-S22 standard method [29].

The samples of S. aureus, S. pyogenes, E. coli, and P. aeruginosa were retrieved from the -20°C freezer and cultured on MHA medium. After one day of incubation at 37°C, a few colonies from each bacterium's culture medium were picked with a loop and incubated in 5 ml of MHB medium overnight at 37°C and a speed of 150 rpm. Subsequently, a dilution equivalent to 0.5 McFarland was prepared from each bacteria sample using sterile MHB medium. These dilutions were further diluted 150 times with sterile physiological serum. Following this, 100 μl of sterile MHB culture medium was added to each well of the microtiter plate, and a dilution series ranging from 48-250 μg/ml of nanoparticles (from a 1000 μg/ml concentration) was prepared in each row of the plate (10 wells).

Next, the McFarland 0.5 suspension, diluted 150 times, was added to each well with a volume of 100 μl. Wells 11 and 12 served as controls for bacterial growth (positive control) and sterility of the growth medium (negative control), respectively. Three repetitions were conducted for each type of nanoparticle. Following the incubation period (24 hours at 37°C), the bacterial growth in the wells was observed. The lowest dilution of nanoparticles that inhibited bacterial growth was identified as the MIC. To determine the Minimum Bacteriocidal Concentration (MBC), bacteria from wells without turbidity were cultured in the amount of 10 μl on MHA medium and incubated at 37°C for 24 hours.

3. Characterization

X-ray diffraction (XRD) patterns of silver and iron ferrite nanoparticles and their nanocomposites were recorded at ambient temperature over a 2θ range of 10°–80° using a PANalytical X'Pert PRO MPD, a multi-purpose X-ray diffraction system with Cu Kα radiation at a wavelength of

λ=1.5405 Å. Fourier transform infrared (FT-IR) spectroscopy was performed with a PerkinElmer FTIR 1650. Before capturing the spectra, the samples were compressed by placing them on a Universal ATR Sampling Accessory. The microstructures and elemental analysis of the nanomaterials were examined using field emission scanning electron microscopy (FESEM) and electron dispersive X-ray analysis (EDAX), utilizing a FEI/Philips XL-30.

3.1. Statistical Analysis

Significant differences were determined through one-way analysis of variance (ANOVA) with pairwise comparisons conducted using Tukey's test. A p-value of ≤0.05 was considered statistically significant. Prism 5 and Minitab 17 software were utilized for the statistical analysis.

4. Results and Discussion

4.1. Structural Properties of AgFe₂O₄ and Fe₃O₄ Nanoparticles, and their Nanocomposites

In Figure 1a, the XRD spectrum of AgFe₂O₄ nanoparticles and their nanocomposites exhibited reflection planes, specifically (012), (220), (310), (311), (321), (411), (421), (122), (520), and (620) at 2θ angles of 24.35°, 33.06°, 35.62°, 37.94°, 44.29°, 49.41°, 54.13°, 62.58°, 64.43°, and 77.37°, respectively. These reflection planes confirmed the cubic phase of the synthesized nanoparticles, validating the formation of AgFe₂O₄ nanoparticles [30]. Additionally, peaks at 2θ angles of 27.90°, 30.2°, 53°, and 61.15° corresponded to (006), (101), and (110) planes of AgFeO₂ nanoparticles with a face-centered cubic crystalline structure (ICCD:01-075-2147) [31]. Furthermore, in the XRD pattern of AgFe₂O₄/SiO₂/Passiflora Caerulea nanocomposites, a broad peak between 2θ angles of 17.8° and 25° indicated the presence of an amorphous SiO₂ layer on AgFe₂O₄ nanoparticles (Figure 1a) [32]. Similarly, peaks at 2θ angles of 32.4°, 36.7°, and 54.1° were respectively associated with (111), (200), and (220) planes of Ag₂O with a face-centered cubic crystalline structure (ICCD: 01-076-1393) [33]. In Figure 1b, distinctive diffraction peaks were observed at 18.31°, 30.12°, 35.48°, 37.11°, 43.12°, 47.21°, 53.50°, 57.03°, 62.62°, 65.85°, and 71.05° in both Fe₃O₄ and Fe₃O₄/SiO₂/Passiflora Caerulea nanocomposites. Comparing these peaks with standard data revealed that they respectively corresponded to the (111), (220), (311), (222), (400), (331), (422), (511), (440), (531), and (620) reflections of face-centered cubic (FCC) Fe₃O₄.

Moreover, a broad peak at 20–30 of 2θ indicating SiO₂ was visible in both Fe₃O₄ and Fe₃O₄/SiO₂/Passiflora Caerulea nanocomposites, confirming the amorphous nature of the coated SiO₂ shell as shown in Figure 1b [34].
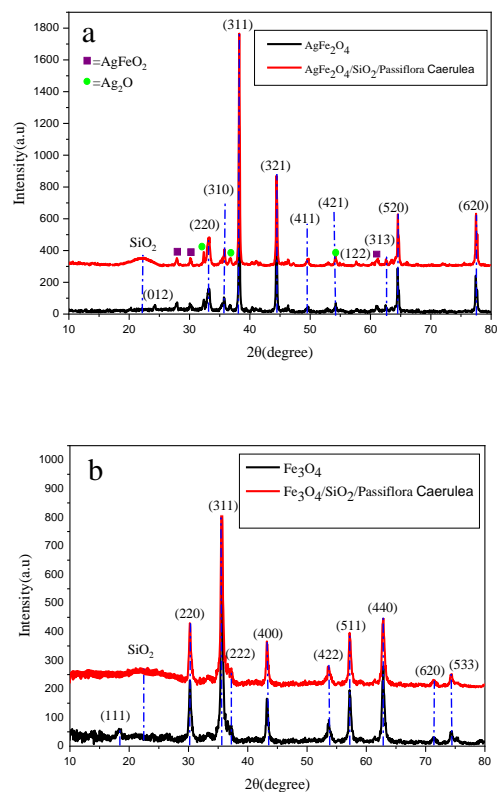
Fig. 1. (a) The XRD patterns of the AgFe₂O₄ nanoparticles and AgFe₂O₄/SiO₂/ Passiflora Caerulea nanocomposite(b) Fe₃O₄ nanoparticles and Fe₃O₄/SiO₂/Passiflora Carulea nanocomposites calcined at 550 °C.

4.2. FT-IR analysis

The FTIR spectra of AgFe₂O₄ and Fe₃O₄ nanoparticles and their nanocomposites are presented in Figure 2. FTIR is a suitable technique for studying chemical adsorption or interactions. The characteristic absorption peak at 455 cm⁻¹ in Figure 2a to 2d is attributed to the Fe-O structure [35]. In the low-energy region, two peaks at 480-570 cm⁻¹ are related to Fe-O vibrations [36]. The Ag-O bond vibration band is observed at 622 cm⁻¹ [37]. The stretching and bending vibrations of O-Si-O are attributed to the bands at 1102 and 790 cm⁻¹ for silica-coated magnetic NPs, respectively (Figure 2b and 2d) [38]. An absorption band at 564.85 cm⁻¹ is linked to the stretching vibrations of Si-O-Fe. After the silica coating, Fe₃O₄/SiO₂/Passiflora Caerulea microspheres show new bands centered around 798 cm⁻¹ and 1080-1100 cm⁻¹ [12, 39]. Additionally, small peaks around 1200-1800 cm⁻¹ are related to the presence of carboxyl and carbonyl groups in the samples. Peaks near 2924-2855 cm⁻¹ can also be associated with the asymmetric and symmetric vibrations of C-H, respectively [40, 41]. A high concentration of PVP results in traces of organic materials at 1280 cm⁻¹, associated with C-N stretching vibration. The most notable peak assigned to PVP appears around 1477 cm⁻¹, corresponding to the stretching mode of H-C-H with weak intensity [42]. Other bands present could be attributed as follows: peaks at 3440 and 1620 cm⁻¹ demonstrate the presence of adsorbed water [43].
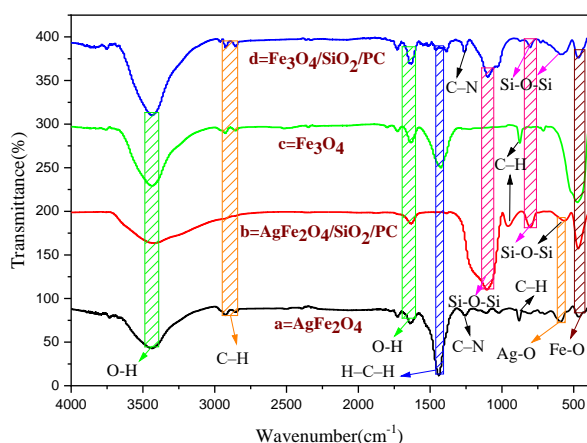
Fig. 2. The FT-IR spectra of AgFe$_2$O$_4$ nanoparticles, (b) AgFe$_2$O$_4$/SiO$_2$/ Passiflora Caerulea nanocomposites, (c) Fe$_3$O$_4$ nanoparticles and (d) Fe$_3$O$_4$/SiO$_2$/ Passiflora Caerulea nanocomposites calcined at 550 °C.

4.3. FE-SEM Analysis

The FE-SEM analysis images shown in Figure 3 depict the morphological features of the synthesized nanoparticles and their nanocomposites. Images in Figures 3a and 3b respectively correspond to AgFe$_2$O$_4$ nanoparticles and AgFe$_2$O$_4$/SiO$_2$/Passiflora Caerulea nanocomposites, revealing lattice-like structures, confirming the preparation conditions discussed earlier. Moving to image Figure 3c, representing Fe$_3$O$_4$, the lattice-like structure is more pronounced compared to AgFe$_2$O$_4$ nanoparticles in Figure 3a. Figure 3d corresponds to Fe$_3$O$_4$/SiO$_2$/Passiflora Caerulea nanocomposites, where the lattice reveals the semi-porous structure of the Fe$_3$O$_4$ nanoparticles, beneficial for cell adhesion and with promising biomedical applications [44]. This structure results from the interaction between magnetic nanoparticles, the small size of the particles, and the nanometer-scale features on their surfaces, increasing the surface energy of the particles. The magnetic properties may lead to particle aggregation. Additionally, spherical nanopowder particles are highly prone to agglomeration. The ionic distance between cations is reduced at B-B sites, leading to nanoparticle condensation [45].

4.4. EDX Analysis

This analysis was conducted to identify the formation compounds and their relative proportions in the current mixtures, as shown in Figures 4a to 4d. EDX spectra confirmed the presence of Ag (Figures 4a and 4b) and Fe (Figures 4c and 4d) through robust signal energy peaks for silver atoms within the range of 3 keV [46]. Fe, O, C, Si, and other individual elements were also detected due to surface plasmon resonance in 22.11% of Ag. Additionally, it displays elemental maps of all the elements separately, indicating homogeneous distribution in the structure.

4.5. Determining the MIC of the Studied Bacteria by Broth Microdilution Method

Four strains of S. aureus, S. pyogenes, E. coli, and P. aeruginosa were utilized to determine the Minimum Inhibitory Concentration (MIC) of nanoparticles. The MIC was defined as the lowest concentration of nanoparticles at which turbidity indicating bacterial growth was not observed. Table 1 presents the MIC investigation results of AgFe$_2$O$_4$ and Fe$_3$O$_4$ nanoparticles and their nanocomposites against the studied bacteria in the Mueller-Hinton broth (MHB) medium. Figure 5 illustrates a 96-well microplate displaying the MIC outcomes of silver ferrite nanoparticles and their nanocomposites on the growth of E. coli.

The results indicate that the inhibitory effect of silver ferrite nanoparticles and their nanocomposites on the growth of Gram-Positive bacteria is significantly higher than that of the silver ferrite nanoparticles synthesized through the thermal method (p≤ 0.05). Moreover, AgFe$_2$O$_4$/SiO$_2$/Passiflora Caerulea nanocomposites demonstrated a significant antibacterial impact on Gram-Positive bacterial growth compared to AgFe$_2$O$_4$ nanoparticles (p≤ 0.05). Table 1 displays the results of the MIC investigation of AgFe$_2$O$_4$, Fe$_3$O$_4$, and their nanocomposites for the studied bacteria in the MHB medium. The results also show that the inhibitory capacity of the iron ferrite nanocomposite to suppress the growth of Gram-negative bacteria is significantly higher than that of the synthesized iron ferrite nanoparticle (p≤0.05).

4.6. Results of MBC Determination of Bacterial Cells

Following MIC determination, wells without turbidity were cultured on Mueller Hinton Agar medium, and the results were analyzed after 24 hours. The lowest concentration that caused the death of 99.9% of the inoculated bacteria was designated as the minimum bactericidal concentration (MBC).

According to the findings, the bactericidal concentration of the silver ferrite nanocomposite on both Gram-Negative and Gram-Positive bacteria aligned with their growth inhibitory concentration. Essentially, the silver ferrite nanocomposite exhibited equivalent inhibitory and bactericidal concentrations, a characteristic not observed in the thermal silver ferrite nanoparticle.

As indicated by the results, the bactericidal concentration of iron ferrite nanocomposite, like silver ferrite nanoparticles, on gram-negative and gram-positive bacteria was equal to their growth inhibitory concentration. In other words, the iron ferrite nanocomposite also exhibited the same inhibitory and bactericidal concentrations, whereas this property was not observed in the iron ferrite nanoparticle in S. pyogenes. The antibacterial activity of nanoparticles depends on several physicochemical properties such as solubility, shape, size, and the capability of forming free biocidal metal ions. Smaller nanoparticles demonstrate greater antibacterial activity compared to larger ones. Gram-positive and Gram-negative bacteria differ in terms of cell membrane

components and cell wall structure, leading to different absorption pathways for nanoparticles. The sensitivity of bacteria to nanoparticles also relies on their biochemical composition since different nanoparticles target different biomolecules. Furthermore, fast-growing bacteria are more sensitive to nanoparticles or antibiotics compared to slow-growing bacteria, which may be attributed to the variable expression of stress response genes between fast-growing and slow-growing bacteria. Studies have indicated that the antibacterial effects of nanoparticles on Gram-positive bacteria exceed their effects on Gram-negative bacteria. This disparity may be linked to the non-porous nature of the cell walls of Gram-negative bacteria, which serve as barriers to the entry of nanoparticles. In contrast, the relatively porous cell walls of gram-positive bacteria have covalent bonds with neighboring proteins and components that permit the penetration of foreign molecules [47]. In the present study, it was observed that Gram-negative bacteria exhibited greater sensitivity to nanoparticles compared with Gram-positive bacteria. The response of bacteria to nanoparticles can be attributed to the physicochemical characteristics of nanoparticles, cell wall structure, and the expression of bacterial stress genes.
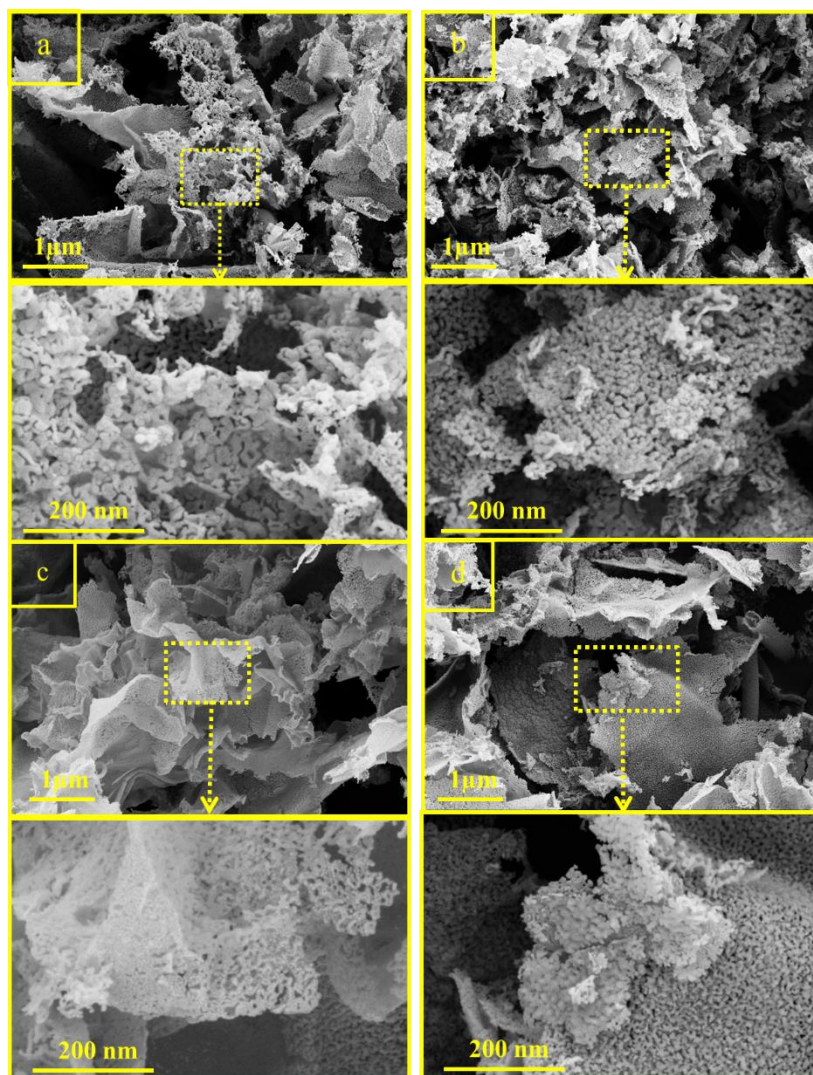
Fig. 3. (a)The FESEM images of $AgFe_2O_4$ nanoparticles, (b) $AgFe_2O_4/SiO_2/$ Passiflora Caerulea nanocomposites, (c) Fe_3O_4 nanoparticles and (d) $Fe_3O_4/SiO_2/$ Passiflora Caerulea nanocomposites calcined at 550 °C.
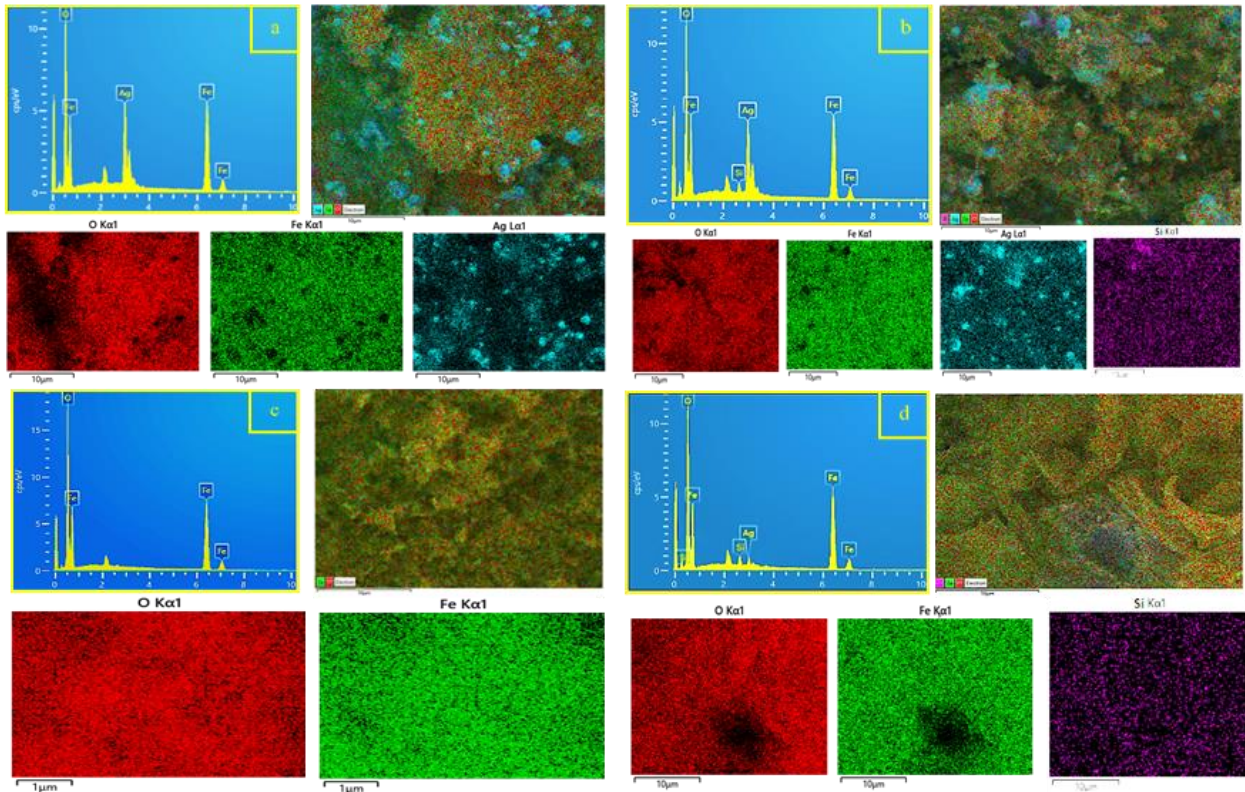
Fig. 4. EDX analysis, and elemental mapping analysis of AgFe$_2$O$_4$ nanoparticles, (b) AgFe$_2$O$_4$/SiO$_2$/ Passiflora Caerulea nanocomposites, (c)Fe$_3$O$_4$ nanoparticles and (d) Fe$_3$O$_4$/SiO$_2$/ Passiflora Caerulea nanocomposites calcined at 550 °C.
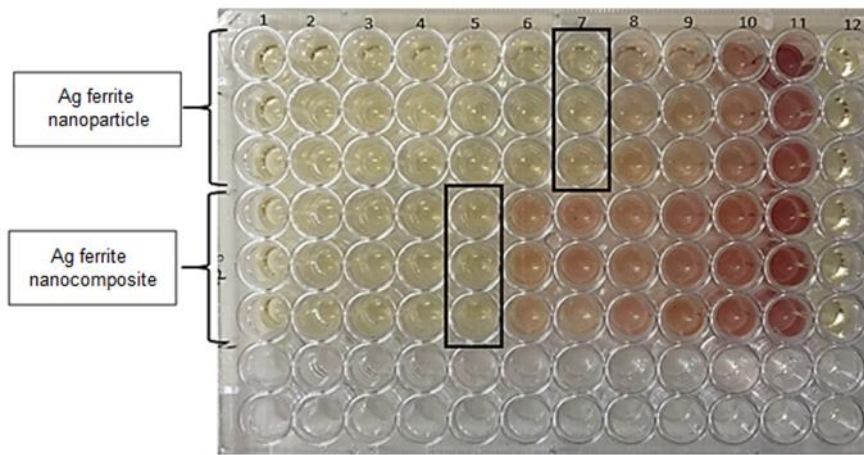
Fig. 5. 96-well microplate sample of AgFe$_2$O$_4$ nanoparticles and AgFe$_2$O$_4$/SiO$_2$/ Passiflora Caerulea nanocomposites MIC on E.coli bacteria. Well number 7 shows a concentration of 3.9 µg/ml and well number 5 shows a concentration of 15.62 µg/ml, which were reported as the MIC AgFe$_2$O$_4$ nanoparticles and AgFe$_2$O$_4$/SiO$_2$/ Passiflora Caerulea nanocomposites.

Table 1. The MIC of the investigated of AgFe$_2$O$_4$ and Fe$_3$O$_4$, and their nanocomposites for the studied bacteria in the MHB medium.

Nanoparticles	concentration range (µg/mL)	MIC (µg/mL)			
		S.pyogenes	*S.aureus*	*E.coli*	*P.aeruginosa*
AgFe$_2$O$_4$ nanoparticles	0.48- 250	31.25	62.5	15.62	62.5
AgFe$_2$O$_4$/SiO$_2$/ Passiflora Caerulea nanocomposites	0.48- 250	31.25	31.25	3.9	15.62
Fe$_3$O$_4$ nanoparticles	0.48- 250	250	125	62.5	125
Fe$_3$O$_4$/SiO$_2$/ Passiflora Caerulea nanocomposites	0.48- 250	125	62.5	15.62	31.25

Table 2. The MBC of the investigated nanoparticles of $AgFe_2O_4$ and Fe_3O_4, and their nanocomposites for the studied bacteria on the MHA medium.

Nanoparticles	concentration range ($\mu g/mL$)	MBC ($\mu g/mL$)			
		S.pyogenes	*S.aureus*	*E.coli*	*P.aeruginosa*
$AgFe_2O_4$ nanoparticles	0.48- 250	250	125	31.25	125
$AgFe_2O_4/SiO_2/$ Passiflora Caerulea nanocomposites	0.48- 250	MBC=MIC	MBC=MIC	MBC=MIC	MBC=MIC
Fe_3O_4 nanoparticles	0.48- 250	MBC>MIC	MBC=MIC	MBC=MIC	MBC=MIC
$Fe_3O_4/SiO_2/$ Passiflora Caerulea nanocomposites	0.48- 250	MBC=MIC	MBC=MIC	MBC=MIC	MBC=MIC

5. Conclusion

In this study, silver and iron ferrite nanoparticles and their nanocomposites were synthesized to investigate their microbiological properties. The structural properties of the materials were examined using various techniques such as XRD for precise crystal analysis and phase identification, FTIR for the identification of organic compounds present, FESEM for high-resolution surface imaging, and EDX analysis for determining the elemental composition of the samples. Additionally, silicon dioxide (SiO_2) nanoparticles were utilized in the nanocomposites to enhance their stability and dispersion, potentially contributing to the observed superior antimicrobial activity. Subsequently, the antimicrobial properties were investigated through MIC and MBC methods. The $Fe_3O_4/SiO_2/$Passiflora Caerulea nanocomposites, exhibited enhanced antimicrobial activity compared to the silver and iron ferrite nanoparticles alone, as determined by the antimicrobial results. These novel findings highlight the synergistic antimicrobial effects of silver, iron ferrite, and SiO_2 nanocomposites in conjunction with Passiflora Caerulea plant extracts. Overall, these advancements hold promising implications for the medical field in combatting bacterial infections and drug-resistant pathogens, presenting a potential avenue for the development of effective antimicrobial agents with a multifaceted approach.

Acknowledgements

Conflicts of Interest

The author declares that there is no conflict of interest regarding the publication of this article.

References

[1] Santhoshkumar, J., Sowmya, B., Kumar, S. V., and Rajeshkumar, S., 2019. Toxicology evaluation and antidermatophytic activity of silver nanoparticles synthesized using leaf extract of Passiflora caerulea. *South African Journal of Chemical Engineering*, *29*, 17-23.

[2] Alshameri, A. W., & Owais, M., 2022. Antibacterial and cytotoxic potency of the plant-mediated synthesis of metallic nanoparticles Ag NPs and ZnO NPs: A review. *OpenNano*, *8*, 100077.

[3] Montiel Schneider, M. G., Martín, M. J., Otarola, J., Vakarelska, E., Simeonov, V., Lassalle, V., and Nedyalkova, M., 2022. Biomedical applications of iron oxide nanoparticles: current insights progress and perspectives. *Pharmaceutics*, *14*(1), 204.

[4] Li, W. R., Xie, X. B., Shi, Q. S., Zeng, H. Y., Ou-Yang, Y. S., and Chen, Y. B., 2010. Antibacterial activity and mechanism of silver nanoparticles on Escherichia coli. *Applied microbiology and biotechnology*, *85*, 1115-1122.

[5] Pakravan, N., Shayani-Jam, H., Beiginejad, H., anf Tavafi, H., 2021. A green and efficient synthesis of novel caffeic acid derivatives with Meldrum's acid moieties as potential antibacterial agents. *Journal of the Iranian Chemical Society*, *18*, 2679-2688.

[6] Aritonang, H. F., Koleangan, H., and Wuntu, A. D., 2019. Synthesis of silver nanoparticles using aqueous extract of medicinal plants'(Impatiens balsamina and Lantana camara) fresh leaves and analysis of antimicrobial activity. *International journal of microbiology*, *2019*.

[7] Gong, P., Li, H., He, X., Wang, K., Hu, J., Tan, W., ... and Yang, X., 2007. Preparation and antibacterial activity of Fe3O4@ Ag nanoparticles. *Nanotechnology*, *18*(28), 285604.

[8] Lagashetty, A., Pattar, A., and Ganiger, S. K., 2019. Synthesis, characterization and antibacterial study of Ag doped magnesium ferrite nanocomposite. *Heliyon*, *5*(5).

[9] Muthukumar, H., Palanirajan, S. K., Shanmugam, M. K., and Gummadi, S. N., 2020. Plant extract mediated synthesis enhanced the functional properties of silver ferrite nanoparticles over chemical mediated synthesis. *Biotechnology Reports*, *26*, e00469.

[10] Sivakumar, S. R., Manimaran, K., Govindasamy, M., Alzahrani, F. M., and Alsaiari, N. S., 2023. Green synthesis and characterization of CuO nanoparticles using Halymenia dilatata extract and its evaluation of antimicrobial, anticancer activity. *Biomass Conversion and Biorefinery*, 1-10.

[11] Jamzad, M., and Kamari Bidkorpeh, M.,(2020. Green synthesis of iron oxide nanoparticles by the aqueous extract of Laurus nobilis L. leaves and evaluation of the antimicrobial activity. *Journal of nanostructure in Chemistry*, *10*(3), 193-201.

[12] Khezripour, A. R., Souri, D., Tavafi, H., and Ghabooli, M. 2019. Serial dilution bioassay for the detection of antibacterial potential of ZnSe quantum dots and their

Fourier transform infra-red spectroscopy. *Measurement*, *148*, 106939.

[13] Kamalianfar, A., Naseri, M., Abdala, A. A., and Jahromi, S. P., 2021. Hierarchical sphere-like ZnO–CuO grown in a controlled boundary layer for high-performance H2S sensing. *Journal of Electronic Materials*, *50*(9), 5168-5176.

[14] Naseri, M. G., Sadrolhosseini, A. R., Dehzangi, A., Kamalianfar, A., Saion, E. B., Zamiri, R., ... and Majlis, B. Y., 2014. Silver nanoparticle fabrication by laser ablation in polyvinyl alcohol solutions. *Chinese Physics Letters*, *31*(7), 077803.

[15] Anajafi, Z., Naseri, M., and Neri, G., 2019. Optical, magnetic and gas sensing properties of LaFeO 3 nanoparticles synthesized by different chemical methods. *Journal of Electronic Materials*, *48*, 6503-6511.

[16] Hedayati, K., Azarakhsh, S., Saffari, J., and Ghanbari, D., 2017. Magnetic and Photo-catalyst CoFe 2 O 4-CdS Nanocomposites: Simple Preparation of Ni, Co, Zn or Ag-Doped CdS Nanoparticles. *Journal of Materials Science: Materials in Electronics*, *28*, 5472-5484.

[17] Hedayati, K., and Nabiyouni, G., 2014. Surface roughness analysis and magnetic property studies of nickel thin films electrodeposited onto rotating disc electrodes. *Applied Physics A*, *116*, 1605-1612.

[18] Dehzangi, A., Larki, F., Naseri, M. G., Navasery, M., Majlis, B. Y., Wee, M. F. R., ... and Saion, E., 2015. Fabrication and simulation of single crystal p-type Si nanowire using SOI technology. *Applied Surface Science*, *334*, 87-93.

[19] Kamalianfar, A., and Naseri, M. G., 2019. Effect of boundary layer thickness on ammonia gas sensing of Cr2O3-decorated ZnO multipods. *Applied Physics A*, *125*(5), 370.

[20] Laouini, S. E., Bouafia, A., Soldatov, A. V., Algarni, H., Tedjani, M. L., Ali, G. A., and Barhoum, A., 2021. Green synthesized of Ag/Ag2O nanoparticles using aqueous leaves extracts of Phoenix dactylifera L. and their azo dye photodegradation. *Membranes*, *11*(7), 468.

[21] Ghasemi, R., Naseri, M., Souri, D., and Kamalianfar, A., 2022. Structural and physical properties of Co1-xCdxFe2O4/SiO2 nanocomposites. *Progress in Physics of Applied Materials*, *2*(2), 147-156.

[22] Zhang, X. F., Liu, Z. G., Shen, W., and Gurunathan, S., 2016. Silver nanoparticles: synthesis, characterization, properties, applications, and therapeutic approaches. *International journal of molecular sciences*, *17*(9), 1534.

[23] Sadighian, S., Sharifan, K., Khanmohammadi, A., and Rohani, M. K., 2021. A facile synthesis of Fe3O4@ SiO2@ zno for curcumin delivery. *Biointerface Res. Appl. Chem*, *12*, 7994-8002.

[24] Cheraghi, M., Lorestani, B., Zandipak, R., and Sobhanardakani, S., 2022. GO@ Fe3O4@ ZnO@ CS nanocomposite as a novel adsorbent for removal of doxorubicin hydrochloride from aqueous solutions. *Toxin Reviews*, *41*(1), 82-91.

[25] Chen, L., and Liang, J., 2020. An overview of functional nanoparticles as novel emerging antiviral therapeutic agents. *Materials Science and Engineering: C*, *112*, 110924.

[26] Avila, J. E. N. N. Y., Jiménez, A. N. G. E. L., Méndez, J. O. N. H., and Murillo, E. L. I. Z. A. B. E. T. H., 2021. Chemical and biological potential of passiflora vitifolia fruit byproducts collected in the Colombian central Andes. *Asian Journal of Pharmaceutical and Clinical Research*, 182-189.

[27] Naseri, M. G., Halimah, M. K., Dehzangi, A., Kamalianfar, A., Saion, E. B., and Majlis, B. Y., 2014. A comprehensive overview on the structure and comparison of magnetic properties of nanocrystalline synthesized by a thermal treatment method. *Journal of Physics and chemistry of solids*, *75*(3), 315-327.

[28] Salimi, N., Mohammadi-Manesh, E., Ahmadvand, N., Danafar, H., and Ghiasvand, S., 2023. Curcumin-Loaded by Fe3O4/GO and Fe3O4/ZnO/GO Nanocomposites for Drug Delivery Applications: Synthesis, Characterization and Anticancer Assessment. *Journal of Inorganic and Organometallic Polymers and Materials*, 1-16.

[29] James, S., Lewis, I., 2022. Performance standards for antimicrobial susceptibility testing (33 Eds), CLSI M100-S22-U, 2023.

[30] Singh, H., Rajput, J. K., Dogra, N., Jain, G., Gupta, A., and Garg, S., 2021. A novel sucrose chelated visible-light sensitive AFO NPs: preparation, characterization, photocatalytic activity, and reaction mechanism. *Journal of the Australian Ceramic Society*, *57*, 835-848.

[31] Naderi, E., Aghajanzadeh, M., Zamani, M., Hashiri, A., Sharafi, A., Kamalianfar, A., ... and Danafar, H., 2020. Improving the anti-cancer activity of quercetin-loaded AgFeO2 through UV irradiation: Synthesis, characterization, and in vivo and in vitro biocompatibility study. *Journal of Drug Delivery Science and Technology*, *57*, 101645.

[32] Esmaeilpour, M., Sardarian, A. R., and Firouzabadi, H., 2018. Theophylline supported on modified silica-coated magnetite nanoparticles as a novel, efficient, reusable catalyst in green one-Pot synthesis of spirooxindoles and phenazines. *ChemistrySelect*, *3*(32), 9236-9248.

[33] Fayyadh, A. A., and Jaduaa Alzubaidy, M. H., 2021. Green-synthesis of Ag2O nanoparticles for antimicrobial assays. *Journal of the Mechanical Behavior of Materials*, *30*(1), 228-236.

[34] Mazhari, M. P., and Hamadanian, M., 2018. Preparation and characterization of Fe3O4@ SiO2@ TiO2 and Ag/Fe3O4@ SiO2@ TiO2 nanocomposites for water treatment: process optimization by response surface methodology. *Journal of Electronic Materials*, *47*(12), 7484-7496.

[35] Wang, L., Sun, Y., Wang, J., Wang, J., Yu, A., Zhang, H., and Song, D., 2011. Preparation of surface plasmon resonance biosensor based on magnetic core/shell Fe3O4/SiO2 and Fe3O4/Ag/SiO2 nanoparticles. *Colloids and Surfaces B: Biointerfaces*, *84*(2), 484-490.

[36] Babu, C. M., Palanisamy, B., Sundaravel, B., Palanichamy, M., and Murugesan, V., 2013. A novel magnetic Fe3O4/SiO2 core–shell nanorods for the removal of arsenic. *Journal of Nanoscience and Nanotechnology*, *13*(4), 2517-2527.

[37] Laouini, S. E., Bouafia, A., Soldatov, A. V., Algarni, H., Tedjani, M. L., Ali, G. A., and Barhoum, A., 2021. Green synthesized of Ag/Ag2O nanoparticles using aqueous leaves extracts of Phoenix dactylifera L. and their azo dye photodegradation. *Membranes*, *11*(7), 468.

[38] Madhavi, Kumar, M., Ansari, J. R., Kumar, V., Nagar, S., and Sharma, A., 2022. Fe3O4 coated SiO2 magnetic nanoparticles for enhanced antibacterial activity and electrochemical sensing. *Metals*, *12*(12), 2145.

[39] Chi, Y., Yuan, Q., Li, Y., Tu, J., Zhao, L., Li, N., and Li, X., 2012. Synthesis of Fe_3O_4@ SiO2–Ag magnetic nanocomposite based on small-sized and highly dispersed silver

nanoparticles for catalytic reduction of 4-nitrophenol. *Journal of colloid and interface science*, *383*(1).

[40] Chireh, M., Karam, Z. M., Naseri, M., Jafarinejad-Farsangi, S., and Ghaedamini, H., 2022. Synthesis, characterization and cytotoxicity study of graphene/doped ZnO/SiO2 nanocomposites. *Applied Physics A*, *128*(4), 307.

[41] Du, Q., Zhang, W., Ma, H., Zheng, J., Zhou, B., and Li, Y., 2012. Immobilized palladium on surface-modified Fe3O4/SiO2 nanoparticles: as a magnetically separable and stable recyclable high-performance catalyst for Suzuki and Heck cross-coupling reactions. *Tetrahedron*, *68*(18), 3577-3584.

[42] Hashemi, A., Naseri, M., and Chireh, M., 2021. Evaluation of physical properties, mechanism and photocatalytic activities of potassium ferrate nanostructures as an adsorbent for MB dye under UV light. *Applied Physics A*, *127*(10), 743.

[43] Anajafi, Z., Naseri, M., Hashemi, A., and Neri, G., 2023. Structural and photocatalytic properties of CeFeO3 and CeFeO3/GO nanostructures. *Journal of Sol-Gel Science and Technology*, *105*(1), 116-126.

[44] Ahmed, S., and Ikram, S., 2016. Chitosan based scaffolds and their applications in wound healing. *Achievements in the life sciences*, *10*(1), 27-37.

[45] Hashemi, A., Naseri, M., Ghiyasvand, S., Naderi, E., and Vafai, S., 2022. Evaluation of physical properties, cytotoxicity, and antibacterial activities of calcium–cadmium ferrite nanoparticles. *Applied Physics A*, *128*(3), 236.

[46] Santhoshkumar, J., Sowmya, B., Kumar, S. V., and Rajeshkumar, S., 2019. Toxicology evaluation and antidermatophytic activity of silver nanoparticles synthesized using leaf extract of Passiflora caerulea. *South African Journal of Chemical Engineering*, *29*, 17-23.

[47] Lee, N. Y., Ko, W. C., and Hsueh, P. R., 2019. Nanoparticles in the treatment of infections caused by multidrug-resistant organisms. *Frontiers in pharmacology*, *10*, 452171.